Available online at www.sciencedirect.com
ScienceDirect
Trans. Nonferrous Met. Soc. China 28(2018) 1073−1083
Transactions of Nonferrous Metals Society of China
www.tnmsc.cn

Microstructural evolution during unsteady-state horizontal solidification of Al−Si−Mg (356) alloy

J. O. LIMA[1], C. R. BARBOSA[1], I. A. B. MAGNO[1,2], J. M. NASCIMENTO[2], A. S. BARROS[2], M. C. OLIVEIRA[1,2], F. A. SOUZA[1,2], O. L. ROCHA[1,2]

1. Federal Institute of Education, Science and Technology of Pará, IFPA, 66093-220, Belém, PA, Brazil;
2. Federal University of Pará, Institute of Technology, UFPA, 66075-110, Belém, PA, Brazil

Received 30 April 2017; accepted 27 September 2017

Abstract: The increasing demand for reducing vehicle weight in the automotive and aerospace industries has raised the need to develop improved structural aluminum-based alloys. Thus, horizontal solidification experiment with the Al−7%Si−0.3%Mg (mass fraction) alloy was carried out. A water-cooled horizontal directional solidification device was developed and used. Microstructural characterization was carried out using traditional techniques of metallography, optical microscopy and SEM microscopy. The Thermo-Calc software was used to generate the solidification path of the investigated alloy with addition of 0.17% Fe (mass fraction). The effects of the thermal parameters such as the growth rate (V_L), cooling rate (T_C) and solidification local time (t_{SL}) on the formation of the macrostructure and on the dendritic microstructure evolution were evaluated. A columnar to equiaxed transition (CET) was found for V_L and T_C values from 0.82 to 0.98 mm/s and from 1.71 to 2.55 °C/s, respectively. The microstructure was characterized by the measurement of the primary and secondary dendrite arm spacings (λ_1 and λ_2, respectively). Experimental laws of $\lambda_1 = f(V_L, T_C)$ and $\lambda_2 = f(t_{SL})$ were proposed. It is observed that the interdendritic region is composed of the following eutectic mixture: α(Al)+Si+π-$Al_8Mg_3FeSi_6$+θ-Mg_2Si.

Key words: Al−Si−Mg alloy; microstructural transition; dendrite arm spacing; transient heat flow

1 Introduction

Aluminum casting alloys are commonly used in automotive and aerospace industry due to their good casting characteristics, mechanical properties as well as good corrosion resistance and weldability [1−10]. It is known that about 80% of these alloys belong to the Al−Si system. In these alloys, the Si alloying element can reduce shrinkage during solidification, the porosity in castings and the thermal expansion coefficient, improve the weldability, increase the flowability, as well as the solidification cracking and mechanical strength.

Al−Si alloys of 3xxx series, with addition of Mg and/or Cu, are most commonly used in the transportation industry, especially in the manufacture of motor vehicles and aircraft [1−4]. In unmodified alloys, the Si particles have a lamellar morphology, which act as initiators for crack propagation and have a negative influence on ductility. On the other hand, the ductility can be improved by changing the lamellar morphology to a fibrous or spheroidal morphology, by imposing, for example, high growth rate (V_L) and cooling rates (T_C) during solidification, or by the addition of a chemical modifier or by heat treatment, or by a combination of these processes. Coarse and brittle intermetallic phases, such as Al_2Cu and Mg_2Si, can be formed during solidification with low T_C values, promoting deleterious effects on the mechanical properties. However, the increase in T_C results in more refined microstructures and, therefore, better mechanical properties.

It is emphasized that significant progress in the development of theoretical and experimental studies to design mechanical and surface properties as a function of thermal and microstructural parameters of metal alloys has been elaborated, considering the directional solidification technique, both in steady and unsteady state conditions. Thus, theoretical and experimental investigations on the effects of thermal parameters (V_L and T_C) on microstructural evolution in binary aluminum-based alloys [1−21] have been developed

Corresponding author: O. L. ROCHA; E-mail: otavio.rocha@ifpa.edu.br; otvrocha@gmail.com
DOI: 10.1016/S1003-6326(18)64751-X

more than three decades ago and more recently for multicomponent alloys [22−27], all with emphasis on directional solidification.

In the case of theoretical studies on the evolution of the dendritic microstructure in binary alloys [11−16], it is highlighted that only those proposed by HUNT and LU [14] for primary spacings and BOUCHARD and KIRKALDY (BK) [16] for primary and secondary spacings assume solidification in unsteady-state heat flow conditions. On the other hand, for multicomponent alloys, it is known in the literature that the theoretical Rappaz and Boettinger (RB) model [22] has been proposed. In general, these models have presented mathematical expressions that correlate the primary dendrite arm spacing λ_1 and the secondary dendrite arm spacing λ_2 with V_L, T_C and t_{SL}, given by the simplified general formula: (λ_1 and λ_2) = Constant (V_L, T_C and t_{SL})^n, where t_{SL} is the time interval between the passage of liquidus and solidus isotherms by a fixed point in the metal, and n is the exponent. It is observed in BK equations [16] that the exponent (n) assumes to be −1/2 for the primary dendrite arm spacing varying with cooling rate and −2/3 for the secondary dendrite arm spacing varying with grooth rate, i.e., $\lambda_1 \propto T_C^{-1/2}$ and $\lambda_2 \propto V_L^{-2/3}$, respectively. It is known that the HL model, for primary dendritic growth [14], presents a complex mathematical expression, however, its experimental application [2−4,10,17] has shown that the slope of the simulated curve has generated an exponent (n) very close to that proposed by BOUCHARD and KIRKALDY. In the RB model [22], the exponent (n) is equal to 1/3 for variation of the secondary dendritic spacing with the solidification local time, i.e., $\lambda_2 \propto t_{SL}^{1/3}$.

Experimental investigation on microstructural evolution of binary and multicomponent Al−Si-based alloys was developed in literature and Table 1 highlights some of these works, whose results present experimental laws of dendritic growth, represented by power-type mathematical equations, similar to those of the theoretical models [14,16,22].

It is observed in Table 1 that the Al−Si casting

Table 1 Experimental laws of primary and secondary dendritic growth for Al−Si-based alloys

Alloy	Experimental law	Ref.
Al−*X*%Si (mass fraction)	$\lambda_2 = kt_{SL}^{0.43}$, k=15.3, 14, 12.8 and 11.5 for X=3.8, 5.7, 7.5 and 9.7, respectively	[1]
	$\lambda_1 = kT_C^{-0.55}$, k=220 for all compositions $\lambda_2 = kV_L^{-2/3}$, k=32 for X=5, and 26 and 22 for X=7 and 9, respectively	[2]
	$\lambda_1 = kV_L^{-1.1}$, k=90 and 55 for X=3 and 7, respectively $\lambda_1 = kT_C^{-0.55}$, k=245 and 212, for X=3 and 7, respectively	[3,4]
	$\lambda_1 = kV_L^{-0.28}$, k=125.3 for X=3 $\lambda_2 = kV_L^{-0.47}$, k=4.8 for X=3	[6]
	$\lambda_2 = kV_L^{-2/3}$, k=29 for X=3 $\lambda_2 = kT_C^{-1/3}$, k=53 for X=3 $\lambda_2 = kt_{SL}^{1/3}$, k=13.5 for X=3	[27]
Al−*X*%Si−*Y*%Mg (mass fraction)	$\lambda_1 = kV_L^{-1.1}$, k=131 for X=1 and Y=3 $\lambda_1 = kT_C^{-0.55}$, k=126 for X=1 and Y=3 $\lambda_2 = kV_L^{-2/3}$, k=27 for X=1 and Y=3 $\lambda_2 = kT_C^{-1/3}$, k=28 for X=1 and Y=3	[23]
	$\lambda_2 = kt_{SL}^{1/3}$, k=13.3 for X=7 and Y=0.3 $\lambda_2 = kT_C^{-1/3}$, k=39.69 for X=7 and Y=0.3	[24]
Al−*X*%Si−*Y*%Cu (mass fraction)	$\lambda_1 = kT_C^{-1.1}$, k=143 and 306 for upward and horizontal directional solidification, respectively, for X=4 and Y=6 $\lambda_2 = kT_C^{-1/3}$, k=14.6 and 54.2 for upward and horizontal directional solidification, respectively, for X=4 and Y=6	[25]
	$\lambda_2 = kV_L^{-2/3}$, k=25 and 15 for for X=5.5 and 9 and Y=3, respectively $\lambda_2 = kT_C^{-1/3}$, k=41 and 28 for for X=5.5 and 9 and Y=3, respectively	[26]
	$\lambda_2 = kV_L^{-2/3}$, k=16 for X=5.5 and Y=3 $\lambda_2 = kT_C^{-1/3}$, k=37 for X=5.5 and Y=3 $\lambda_2 = kt_{SL}^{1/3}$, k=7.8 for X=5.5 and Y=3	[27]

k is a constant, $\lambda_{1,2}$ in μm; V_L in mm/s, T_C in °C/s and t_{SL} in s

alloys are well studied and there is a lot of knowledge on the influence of alloying elements and solidification thermal parameters on the microstructure evolution. These investigations play a relevant role in designing components and equipment with mechanical properties suitable to the transportation industry. Furthermore, CHEN et al [28] has investigated the correlation among microstructure and heat treatment parameters and composition of Mg element with mechanical properties in Al−7Si−*X*Mg cast alloys. The results showed that more refined microstructures allowed to obtain higher tensile properties after thermal treatment. Thus, this study may contribute to the liquid metal processing in automotive and aerospace industry aiming at designing of a required alloy microstructure, considering a better understanding of the thermal parameters and processes occurring in Al−Si−Mg alloys. In this sense, the main purpose of this paper is to investigate the effects of thermal parameters (V_L, T_C and t_{SL}) on the dendritic microstructure evolution of the Al−7%Si−0.3%Mg (mass fraction) alloy horizontally solidified under transient heat flow as well as to perform a comparative analysis of the experimental λ_2 values theoretically calculated with the Rappaz and Boettinger theoretical model [22]. In addition, the solidification path of the investigated alloy will be determined experimentally and compared with the theoretical predictions obtained by Thermo-Calc software. The obtained results have been compared with others found in literature under different growth conditions.

2 Experimental

Transient horizontal directional solidification (THDS) experiment was carried out with Al−7%Si−0.3%Mg alloy, prepared from the weighing of its high purity Al, Si elements and from a Mg-based alloy, which was inserted into a refractory crucible and introduced into a muffle-type melting furnace. The chemical compositions of the metals and the final investigated alloy are summarized in Table 2. The addition of the Si and Mg alloying elements occurred only after the initial melting of the aluminum solvent. In order to verify the liquidus temperature (T_L), the investigated alloy was thermally characterized by obtaining its experimental solidification path. The horizontal solidification of the alloy was conducted using a water-cooled directional solidification device. Figures 1 and 2 show the schemes of the thermal characterization and complete solidification assembly used in this work, respectively. The horizontal solidification setup was designed to permit heat extraction only through the water-cooled system placed in the lateral mold wall. The stainless steel mold used had a wall thickness of 3 mm, a length of 150 mm, a height of 60 mm, and a width of 60 mm.

In order to determine the thermal parameters (V_L, T_C and t_{SL}), a thermal mapping was carried out in the liquid metal along with the THDS by insertion of thermocouples located at strategic positions from the cooled interface. The thermocouples readings, shown in

Table 2 Chemical compositions of metals and alloys (mass fraction, %)

Specimen	Al	Si	Mg	Fe	Ni	Ca	Ti	Zn	Cu
Al	99.7	0.062	−	0.176	0.006	−	0.009	0.007	−
Si	0.1094	99.596	−	0.3164	0.0102	0.0214	0.0455	−	−
Mg-based alloy	6.981	0.246	91.877	0.001	0.001	−	−	0.631	0.115
Investigated alloy	91.33	7.235	0.336	0.148	0.0048	0.019	0.0054	0.054	0.019

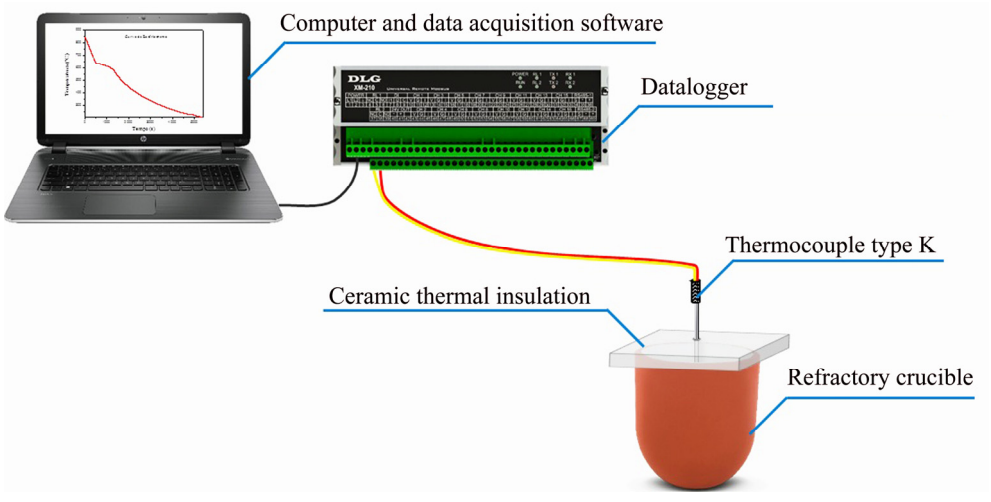

Fig. 1 Scheme of thermal characterization apparatus to obtain solidification path

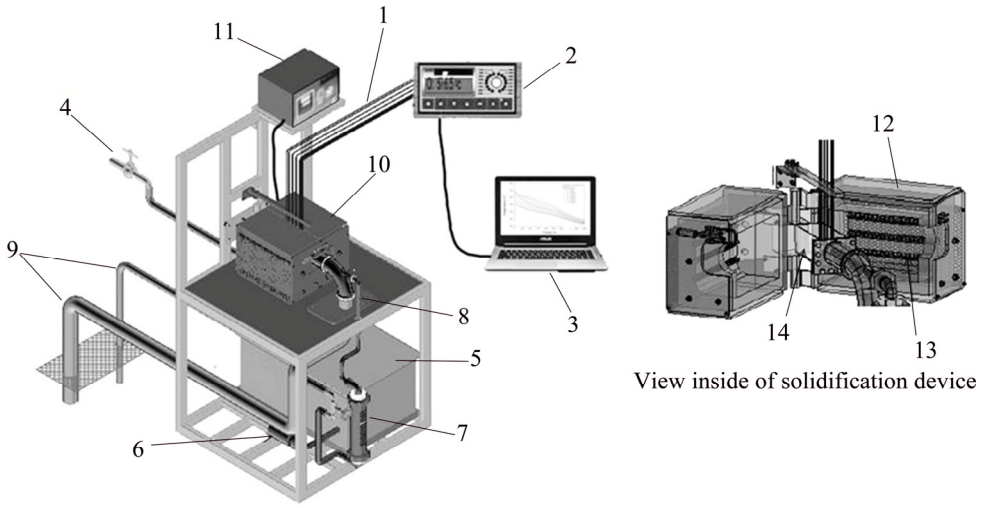

Fig. 2 Experimental complete horizontal directional solidification setup [27]: 1—Thermocouples; 2—Field-logger; 3—Computer and data acquisition software; 4—Feed water; 5—Water container; 6—Water pump; 7—Rotameter; 8—Water inlet; 9—Water outlet; 10—Directional solidification device; 11—Temperature controller; 12—Insulating ceramic shielding; 13—Electric heaters; 14—Rectangular mold (stainless steel mold-inner wall)

Fig. 2 were used to generate a plot of positions from metal/mold interface (P) as a function of time (t) corresponding to the liquidus front passing by each thermocouple. A best fitting curve on these experimental points has generated a power function of position as a function of time, i.e., $P=f(t)$. The derivative of this function with respect to time has yielded values for V_L. The T_C profile was calculated by considering the thermal data recorded immediately after the passing of the liquidus front by each thermocouple. The method used for measuring T_C was detailed by ROCHA et al [17]. The t_{SL} was determined by difference between the time of passage of the solidus isotherm and the time of passage of the liquidus isotherm for a given point in the casting [2].

After the horizontal directional solidification, the resulting ingot was subjected to metallography techniques to characterize and reveal the structure on a macrostructural and microstructural scales. Transverse and longitudinal sections at 2, 4, 6, 10, 15, 20, 30, 40, 50, 60, and 70 mm, whose positions are in the columnar growth region, and 2, 4, 6, 10, 15, 20, 30, 40, 50, 60, 70, 80, 90, 100 and 110 mm, respectively, of the directionally solidified ingot from the metal-mold interface were electropolished and etched with a solution of Keller's reagent (10 mL HF, 15 mL HCl, 25 mL HNO_3, 50 mL H_2O) during 15 s for micrograph examination and measurement of primary and secondary dendrite arm spacings. The method used for measuring λ_1 on the transverse section was the triangle method [8,17]. On the other hand, λ_2 was measured by averaging the distance between adjacent side-branches on the longitudinal section of a primary dendrite [8,17]. Figure 3 schematically shows the techniques used to measure the λ_1 and λ_2 values, respectively.

3 Results and discussion

Figures 4(a) and (b) show the theoretical and experimental solidification paths obtained by the thermal characterization (Fig. 1) and Thermo-Calc software (non-equilibrium conditions), respectively. In order to better represent the inflection points for precipitation of the intermetallic phases, the first derivative of the experimental curve representing the solidification path of the investigated alloy has been determined, as shown in Fig. 4(b). It is observed that the microstructure of investigated 356 alloy in the as-cast state consists of dendritic primary phase of α(Al-rich) solid solution with interdendritic regions of Al−Si eutectic, in which various intermetallic phases such as β-Al_5FeSi, π-$Al_8Mg_3FeSi_6$ and Mg_2Si are present.

The experimental cooling curves referring to the thermal mapping performed on the metal during horizontal solidification are shown in Fig. 5. It has been used to determine the V_L, T_C and t_{SL} values, which are shown in Fig. 6. It is observed that the water-cooled device imposes high growth and cooling rates for positions near the metal/mold interface (cooled interface).

Figure 7 shows the macrograph for the investigated alloy horizontally solidified. It can be seen by the solidification macrostructure that a columnar to equiaxed transition (CET) appears and that CET has

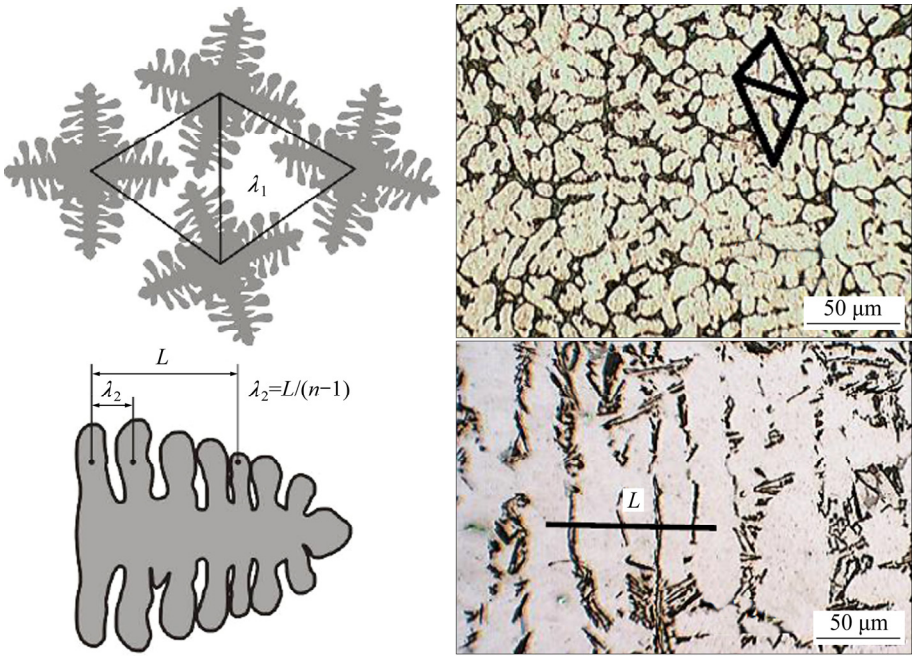

Fig. 3 λ_1 and λ_2 measurement techniques used in this work (n: number of side branches)

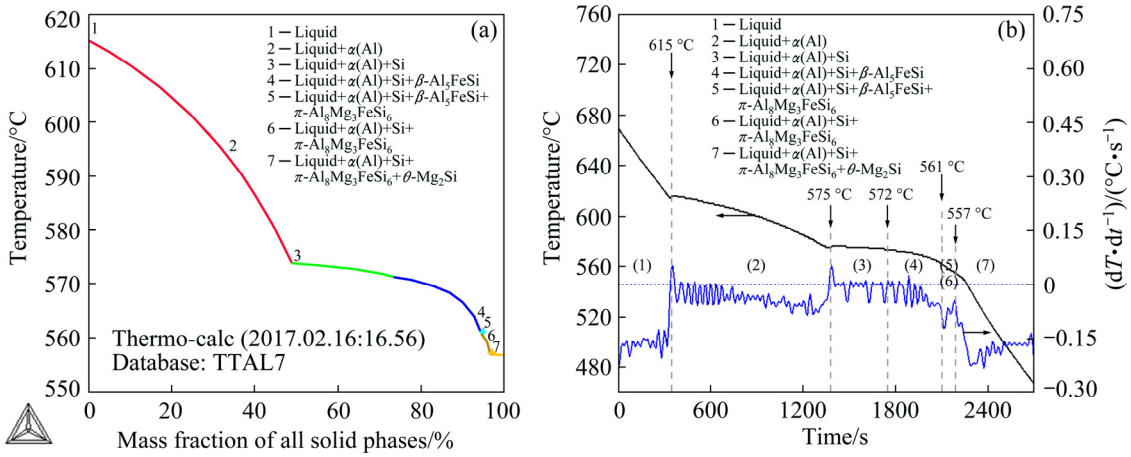

Fig. 4 Theoretical and experimental solidification paths obtained by Thermo-Calc software (a) and experimental methodology (b) of Fig. 1

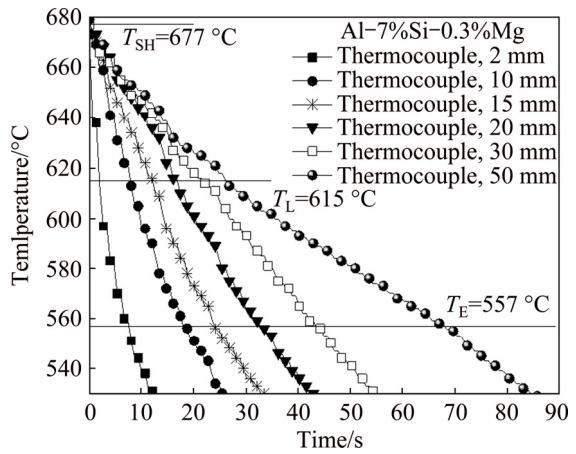

Fig. 5 Experimental cooling curves obtained for six thermocouples inserted in metal (T_{SH}, T_L and T_E are temperatures of superheat, liquidus and eutectic, respectively)

occurred in a zone, represented by a dash line inside Fig. 7, instead of a sharp plane parallel to the metal/mold interface. It is evidenced that the effects of the thermosolutal convection, promoted by the growth direction of the horizontal solidification, have influenced the CET to occur in ranges of V_L (0.82 to 0.98 mm/s) and T_C (1.71 to 2.55 °C/s), as shown by Figs. 6(a) and (b), respectively. The same CET characteristic found in this work has been observed in our recent articles for multicomponent Al−Si based alloys with addition of Cu alloying element [25,27]. Typical longitudinal and transverse microstructures of the Al−7%Si−0.3%Mg alloy along the length of the THDS casting are also shown in Fig. 7. It is observed that the microstructure is characterized by a dendritic morphology along the horizontally solidified ingot, and coarser microstructure

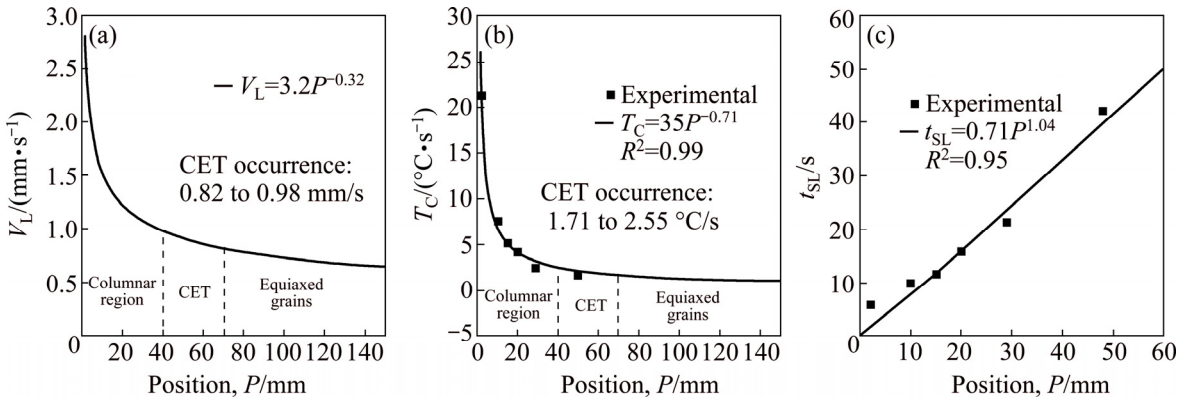

Fig. 6 Thermal parameters resulting from horizontal solidification of Al−7%Si−0.3%Mg alloy (CET is columnar to equiaxed transition): (a) V_L=f(P); (b) T_C=f(P); (c) t_{SL}=f(P)

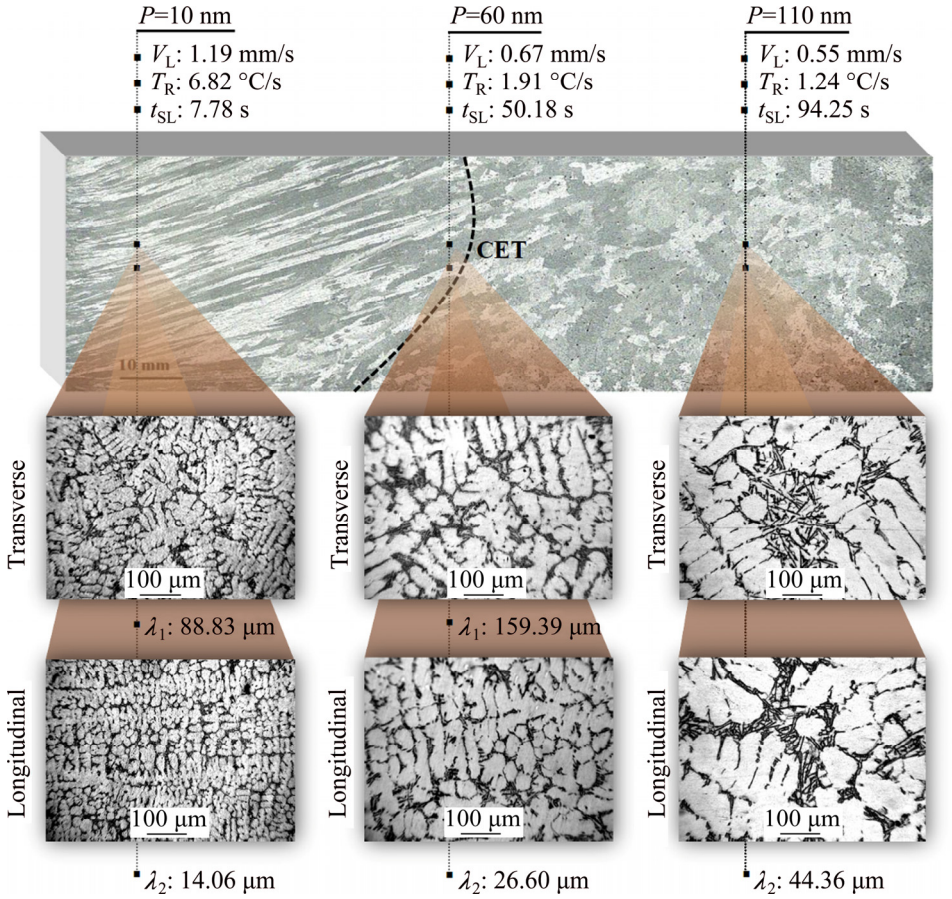

Fig. 7 Macrograph and optical micrographs of transverse and longitudinal sections of Al−7%Si−0.3%Mg alloy ingot (P is position from metal/mold interface)

has been noted for lower V_L and T_C values, i.e., the primary and secondary dendrite arm spacings increase with the distance from the heat-extracting surface. This has been depicted by Figs. 6(a) and (b).

The influence of the thermal parameters has been evaluated in the evolution of the dendritic microstructure. For this end, the V_L, T_C and t_{SL} experimental variations as a function of the liquidus isotherm position (P), presented in Fig. 6, were correlated with the λ_1 and λ_2 values measured in the ingot of horizontally solidified alloy in this work and the results found are consolidated in Figs. 8 and 9.

It is observed from Figs. 8(a) and (b) that the exponents −1.1 and −0.55 have characterized the variation of the primary dendrite arm spacings with the growth rate and the cooling rate, which are absolutely

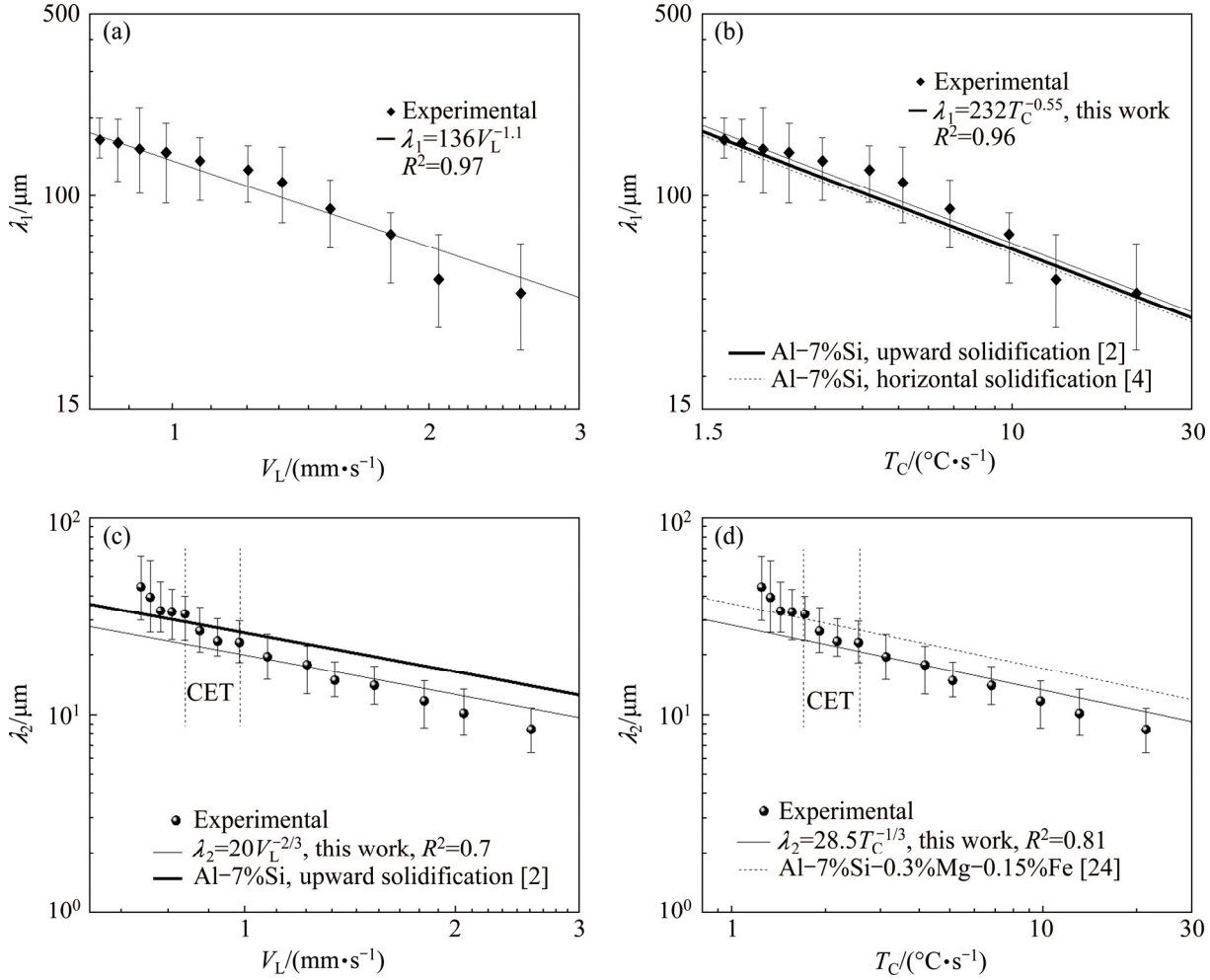

Fig. 8 Experimental laws of dendritic growth for horizontally solidified Al−7%Si−0.3%Mg alloy: (a, b) λ_1; (c, d) λ_2

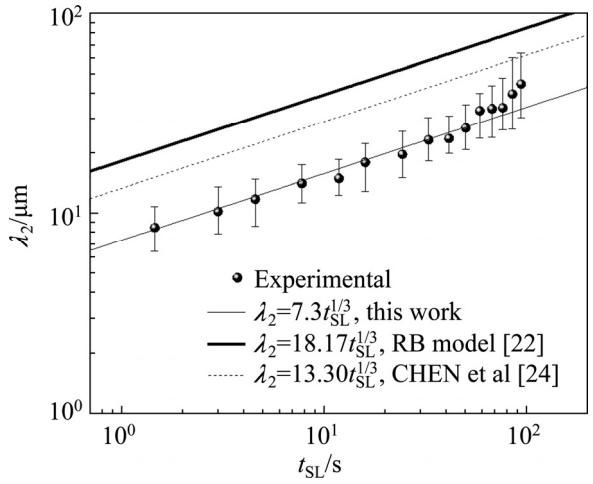

Fig. 9 Comparison between results obtained from this work with those from literature for secondary dendritic spacing

equal to the indices found by PERES et al [2] and CARVALHO et al [4], for the vertical upward and horizontal solidified binary Al−7%Si alloy, respectively. It can be understood that both the addition of the Mg element in the formation of multicomponent Al−7%Si−0.3%Mg alloy and the solidification growth direction (upward and horizontal) do not affect the experimental laws of primary dendritic growth. It is also noted that the λ_2 values of these authors are very close to the values of this work. This should be emphasized that the value of −0.55 is very close to the value of −0.50 proposed by the BK mathematical model [16].

Figures 8(c) and (d) show the dependence of secondary dendrite arm spacing as function of growth rate and cooling rate. It is observed that the exponents −2/3 and −1/3 characterize the experimental growth laws of λ_2 as a function of V_L and T_C for $R^2 \geq 0.7$ (R^2 is the coefficient of determination). On the other hand, a better agreement of the growth laws for λ_2 values measured in the columnar grains region, i.e., for high V_L and T_C values evidenced. In this sense, it can be seen that the CET affects the secondary dendritic growth law for the investigated alloy. It is observed in Fig. 8(c) that the index value of mathematical expression that correlates λ_2 as a function of V_L is equal to −2/3 for both binary Al−7%Si and multicomponent Al−7%Si−0.3%Mg alloys, upward and horizontally solidified, referring to the work

of PERES et al [2] and to this work, respectively. It is evidenced that the solidification direction does not affect the growth law for secondary dendritic spacing and that the exponent proposed in the BK equation ($\lambda_2 \propto V_L^{-2/3}$) seems to be valid for ternary Al-based alloys. Figure 8(d) presents a comparative analysis between the experimental results for multicomponent Al−7%Si−0.3%Mg alloy, obtained under the conditions assumed in this work and those of the work in Ref. [24]. It is observed that the exponent of −1/3 characterizes the λ_2 growth law as a function of T_C, for both investigations. However, it is noted that the experimental law proposed by CHEN et al [24] presents a better approximation in the isotropic growth region, i.e., composed of equiaxed grains.

It is known that RAPPAZ and BOETTINGER (RB) [22] proposed the only predictive model found in the literature for secondary dendritic growth of multicomponent alloys. The general expression is given by

$$\lambda_2 = 5.5(Mt_{SL})^{1/3} \quad (1)$$

$$M = \frac{-\Gamma}{\sum_{j=1}^{n} m_j(1-k_j)(c_{fj}-c_{0j})/D_j} \cdot \ln\left(\frac{\sum_{j=1}^{n} m_j(1-k_j)c_{fj}/D_j}{\sum_{j=1}^{n} m_j(1-k_j)c_{0j}/D_j}\right) \quad (2)$$

where Γ is the Gibbs−Thomson coefficient, c_0 is the alloy composition, m is the liquidus slope, c_f is the eutectic composition, D is the diffusion coefficient in the liquid, and k is the redistribution coefficient. The subscript "j" represents each alloying element and the sum encompasses all the solute elements of the multi-component alloy.

A theoretical−experimental analysis between the results of this work and those calculated from the RB model was performed and the results are shown in Fig. 9. Table 3 shows the thermophysical properties of the investigated alloy, calculated with the Thermo-Calc software. A comparison with the experimental growth law, obtained by CHEN et al [24], has also been developed. It is observed that the λ_2 values calculated by the RB equation overestimate those of this work as well as those of CHEN et al [24]. It should be emphasized that the RB model does not consider a transient heat extraction regime and yet, during its mathematical formulation, the authors have neglected the convective effects that are always present in the horizontal solidification. In spite of these interesting physical characteristics, the literature is scarce on studies dealing with these important effects of solute-induced convection, particularly for multicomponent alloys.

Table 3 Thermo-physical properties of Al−7%Si−0.3%Mg alloy used in Eq. (2)

Property	Value
Liquidus temperature, T_L/°C	615.30
Alloy Gibbs−Thomson coefficient, Γ/(m·K)	7.554×10^{-7}
Magnesium eutectic concentration, c_{Eut}^{Mg}/%	7.510
Silicon eutectic concentration, c_{Eut}^{Si}/%	12.610
Magnesium partition coefficient, k_0^{Mg}	0.222
Silicon partition coefficient, k_0^{Si}	0.110
Silicon liquidus slope, m_L^{Si}/(%·°C^{-1})	6.595
Magnesium liquidus slope, m_L^{Mg}/(%·°C^{-1})	3.520
Magnesium diffusion coefficient in liquid phase, D_L^{Mg} at T_L/(m^2·s^{-1})	9.522×10^{-9}
Silicon diffusion coefficient in liquid phase, D_L^{Si} at T_L/(m^2·s^{-1})	2.80×10^{-9}

The SEM–EDS mapping results for the multicomponent Al−7%Si−0.3%Mg−0.15%Fe alloy are depicted in Fig. 10 for three positions from the metal/mold interface (cooled interface). These images show, for all positions, the presence of the eutectic α(Al)+Si+π-$Al_8Mg_3FeSi_6$+θ-Mg_2Si mixture inside the interdendritic region. It is observed for higher V_L and T_C values that the Fe and Mg solutes are more segregated in the Al−Si eutectic mixture as intermetallic particles (π-$Al_8Mg_3FeSi_6$ and θ-Mg_2Si), dispersed as isolated elements at positions far from the cooled mold. The influence of the V_L and T_C values on the Si particle morphology can also be evidenced, i.e., it is noted that the Si presents the fibrous and lamellar forms at positions closest to and far from the cooled interface where V_L and T_C values are higher and lower, respectively. In order to confirm the phases that form during the solidification, SEM−EDS microanalysis has been performed on the micrograph samples shown in Fig. 10, and one of the results of the EDS compositions is shown in Fig. 11 at P=30 mm.

4 Conclusions

1) The dendritic microstructure has been observed along with the THDS of the Al−7%S−0.3%Mg alloy and the mathematical expressions given by $\lambda_1 = 136V_L^{-1.1}$, $\lambda_1 = 232T_C^{-0.55}$, $\lambda_2 = 20V_L^{-2/3}$, $\lambda_2 = 28.5T_C^{-1/3}$ and $\lambda_2 = 7.3t_{SL}^{1/3}$ characterize the growth experimental laws of the primary and secondary dendrite arm spacings as a function of growth rate, cooling rate and solidification local time, respectively.

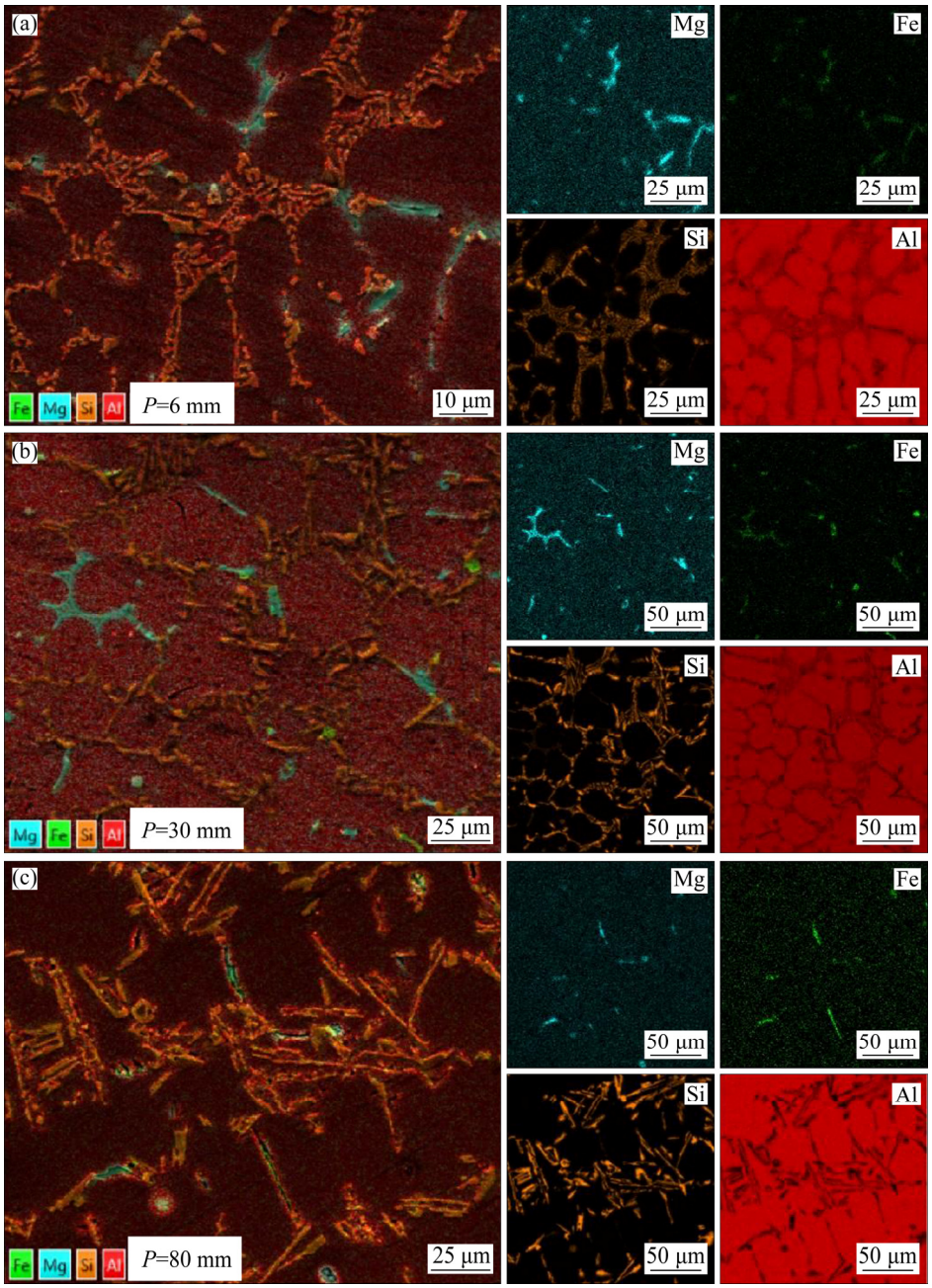

Fig. 10 SEM−EDS images obtained for investigated alloy at three positions in ingot from cooled interface: (a) *P*=6 mm; (b) *P*=30 mm; (c) *P*=80 mm

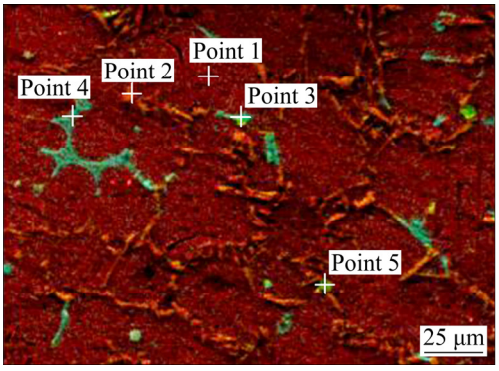

Point No.	Mass fraction/%			
	Al	Si	Mg	Fe
1	98.55	1.42	0.03	−
2	31.79	67.98	0.09	0.14
3	60.84	20.31	7.75	11.1
4	67.84	17.57	8.30	6.29
5	70.08	11.66	0.09	18.18

Fig. 11 EDS spectrum and compositions of Al−7%Si−0.3%Mg−0.15%Fe alloy investigated in this work at *P*=30 mm

2) The λ_2 theoretical values calculated by the RB mathematical expression have overestimated the experimentally determined values of the Al−7%Si−0.3%Mg alloy horizontally solidified in this work.

3) It was observed that the microstructure of the directionally solidified Al−Si−Mg−Fe alloy (356) in this work is composed of an Al-rich matrix (α) surrounded by eutectic mixture with the presence of intermetallic phases of Mg and Fe, forming a mixture of phases in the interdentric regions composed of α(Al)+Si+π-$Al_8Mg_3FeSi_6$+θ-Mg_2Si.

4) The Si particles in the eutectic mixture of the investigated alloy have been characterized to be fibrous and lamellar for high and low V_L and T_C values, respectively and that the intermetallic phases are more concentrated in the interdendritic regions for higher V_L and T_C values.

Acknowledgments

The authors acknowledge the financial support provided by IFPA — Federal Institute of Education, Science and Technology of Pará, UFPA — Federal University of Pará, and CNPq—The Brazilian Research Council (Grants 472745/2013-1, 308784/2014-6 and 302846/2017-4), FAPESPA — Amazon Foundation of Support to Study and Research (Grants ICAAF 064/2016) and CAPES — Coordination of Superior Level Staff Improvement, Brazil.

References

[1] BAMBERGER M, WEISS B Z, STUPEL M M. Heat flow and dendritic arm spacing in chill-cast Al−Si alloys [J]. Materials Science and Technology, 1987, 3: 49−56.

[2] PERES M D, SIQUEIRA C A, GARCIA A. Macrostructural and microstructural development in Al−Si alloys directionally solidified under unsteady-state conditions [J]. Journal of Alloys and Compounds, 2004, 381: 168−181.

[3] CARVALHO D B, GUIMARÃES E C, MOREIRA, A L, MOUTINHO D J, DIAS FILHO J M, ROCHA O L. Characterization of the Al−3wt.%Si alloy in unsteady-state horizontal directional solidification [J]. Materials Research, 2013, 16: 874−883.

[4] CARVALHO D L B, COSTA T A, MOREIRA A L S, SILVA M A P S, DIAS M, MOUTINHO D J C, ROCHA O L. Solidification thermal parameters and dendritic growth during the horizontal directional solidification of Al−7wt.%Si alloy [J]. Magazine Minas School, 2014, 67: 265−270.

[5] MCCARTNEY D G, HUNT J D. Measurements of cell and primary dendrite arm spacings in directionally solidified aluminium alloys [J]. Acta Metallurgica, 1981, 29: 1851−1863.

[6] KAYA H, ÇADIRLI E, GÜNDÜZ M. Dendritic growth in an aluminum−silicon alloy [J]. Journal of Materials Engineering and Performance, 2007, 16: 12−21.

[7] LI X, FAUTRELLE Y, REN Z. Influence of thermoelectric effects on the solid−liquid interface shape and cellular morphology in the mushy zone during the directional solidification of Al−Cu alloys under a magnetic field [J]. Acta Materialia, 2007, 55: 3803−3813.

[8] GÜNDÜZ M, ÇADIRLI E. Directional solidification of aluminium−copper alloys [J]. Materials Science and Engineering A, 2002, 327: 167−185.

[9] SÁ F, ROCHA O L, SIQUEIRA C A, GARCIA A. The effect of solidification variables on tertiary dendrite arm spacing in unsteady-state directional solidification of Sn−Pb and Al−Cu alloys [J]. Materials Science and Engineering A, 2004, 373: 131−138.

[10] CANTÉ M V, SPINELLI J E, CHEUNG N, GARCIA A. The correlation between dendritic microstructure and mechanical properties of directionally solidified hypoeutectic Al−Ni alloys [J]. Metals and Materials International, 2010, 16: 39−49.

[11] KIRKWOOD D H. A simple model for dendritic arm coarsening during solidification [J]. Materials Science and Engineering A, 1985, 73: 1−4.

[12] TRIVEDI R, KURZ W. Dendritic growth [J]. International Materials Reviews, 1994, 39: 49−74.

[13] OKAMOTO T, KISHITAKE K. Dendritic structure in unidirectionally solidified aluminum, tin, and zinc base binary alloys [J]. Journal of Crystal Growth, 1975, 29: 137−146.

[14] HUNT J D, LU S Z. Numerical modeling of cellular/dendritic array growth: Spacing and structure predictions [J]. Metallurgical Transactions A, 1996, 27: 611−623.

[15] KURZ W, FISHER D J. Dendrite growth at the limit of stability: Tip and spacing [J]. Acta Metallurgica, 1981, 29: 11−20.

[16] BOUCHARD D, KIRKALDY J S. Prediction of dendrite arm spacings in unsteady and steady-state heat flow of unidirectionally solidified binary alloys [J]. Metallurgical and Materials Transactions B, 1997, 28: 651−663.

[17] ROCHA O L, SIQUEIRA C A, GARCIA A. Heat flow parameters affecting dendrite spacings during unsteady-state solidification of Sn−Pb and Al−Cu alloys [J]. Metallurgical and Materials Transactions A, 2003, 34: 995−1006.

[18] KAYA H, BÖYÜK U, ÇADIRLI E, MARASLI N. Measurements of the microhardness, electrical and thermal properties of the Al−Ni eutectic alloy [J]. Materials and Design, 2012, 34: 707−712.

[19] KAYA H, BOYUK U, ÇADIRLI E, MARASLI N. Influence of growth rate on microstructure, microhardness and electrical resistivity of directionally solidified Al−7wt%Ni hypoeutectic alloy [J]. Metals and Materials International, 2013, 19: 39−44.

[20] ÇADIRLI E. Effect of solidification parameters on mechanical properties of directionally solidified Al-rich Al−Cu alloys [J]. Metals and Materials International, 2013, 19: 411−422.

[21] BARROS A S, MAGNO I L, SOUZA F A, MOREIRA A L, SILVA M A, ROCHA O L. Measurements of microhardness during transient horizontal directional solidification of Al-rich Al−Cu alloys: Effect of thermal parameters, primary dendrite arm spacing and Al_2Cu intermetallic phase [J]. Metals and Materials International, 2015, 21: 429−439.

[22] RAPPAZ M, BOETTINGER W J. On dendritic solidification of multicomponent alloys with unequal liquid diffusion coefficients [J]. Acta Materialia, 1999, 47: 3205−3219.

[23] BRITO C, COSTA T A, VIDA T A, BERTELLI F, CHEUNG N, SPINELLI J E, GARCIA A. Characterization of dendritic microstructure, intermetallic phases, and hardness of directionally solidified Al−Mg and Al−Mg−Si alloys [J]. Metallurgical and Materials Transactions A, 2015, 46: 3342−3355.

[24] CHEN R, SHI Y F, XU Q Y, LIU B C. Effect of cooling rate on solidification parameters and microstructure of Al−7Si−0.3Mg−0.15Fe alloy [J]. Transactions of Nonferrous Metals Society of China, 2014, 24: 1645−1652.

[25] COSTA T A, MOREIRA A L, MOUTINHO D J, DIAS M, FERREIRA I L, SPINELLI J E, ROCHA O L, GARCIA A. Growth direction and Si alloying affecting directionally solidified structures of Al−Cu−Si alloys [J]. Materials Science and Technology, 2015, 31: 1103−1112.

[26] GOMES L G, MOUTINHO D J, FERREIRA I L, ROCHA O L, GARCIA A. The growth of secondary dendritic arms in directionally solidified Al−Si−Cu alloys: A comparative study with binary Al−Si alloys [J]. Applied Mechanics and Materials, 2015, 719−720: 102−105.

[27] ARAÚJO E C, BARROS A S, KIKUCHI R H, SILVA A P, GONÇALVES F A, MOREIRA A L, ROCHA O L. The role of Si and Cu alloying elements on the dendritic growth and microhardness in horizontally solidified binary and multicomponent aluminum-based alloys [J]. Metallurgical and Materials Transactions A, 2017, 48: 1163−1175.

[28] CHEN R, XUA Q, GUOB H, XIAB Z, WUB Q, LIUA. Correlation of solidification microstructure refining scale, Mg composition and heat treatment conditions with mechanical properties in Al−7Si−Mg cast aluminum alloys [J]. Materials Science and Engineering A, 2017, 685: 391−402.

Al−Si−Mg (356)合金不稳态水平凝固过程中的显微组织演化

J. O. LIMA[1], C. R. BARBOSA[1], I. A. B. MAGNO[1,2], J. M. NASCIMENTO[2], A. S. BARROS[2], M. C. OLIVEIRA[1,2], F. A. SOUZA[1,2], O. L. ROCHA[1,2]

1. Federal Institute of Education, Science and Technology of Pará, IFPA, 66093-220, Belém, PA, Brazil;
2. Federal University of Pará, Institute of Technology, UFPA, 66075-110, Belém, PA, Brazil

摘　要：汽车和航空航天工业对减少运载工具重量的需求不断增加，这就需要发展改良的结构铝基合金。因此，本文作者研究设计 Al−7%Si−0.3%Mg 合金的水平凝固实验。研制并使用水冷式水平定向凝固装置。运用金相、光学显微镜、扫描电镜等传统技术表征材料的显微组织。用 Thermo-Calc 软件模拟含 0.17% Fe(质量分数)合金的凝固路径。研究生长速度(V_L)、冷却速度(T_C)和凝固局部时间(t_{SL})等热力学参数对显微组织形成和枝晶显微组织演化的影响。当 V_L 和 T_C 值分别为 0.82~0.98 mm/s 和 1.71~2.55 °C/s 时，柱状晶向等轴晶转变(CET)。通过测量一次和二次枝晶间距(分别为 λ_1 和 λ_2)对显微组织进行表征。提出实验性定律：$\lambda_{1,2}=f(V_L, T_C)$，$\lambda_2=f(t_{SL})$；并观察到枝晶区包含以下共晶混合物：$\alpha$(Al)+Si+$\pi$-$Al_8Mg_3FeSi_6$+$\theta$-$Mg_2Si$。

关键词：Al−Si−Mg 合金；显微组织演化；枝晶间距； 瞬时热流

(Edited by Wei-ping CHEN)